Russian Journal of Physical Chemistry, Vol. 74, No. 10, 2000, pp. 1702–1710. Translated from Zhurnal Fizicheskoi Khimii, Vol. 74, No. 10, 2000, pp. 1874–1883.

BIOPHYSICAL CHEMISTRY

Kinetic Model of Photosystem II of Higher Green Plants

G. V. Lebedeva*, N. E. Belyaeva*, G. Yu. Riznichenko*, A. B. Rubin*, and O. V. Demin**

* *Faculty of Biology, Moscow State University, Vorob'evy gory, Moscow, 119899 Russia*

** *Belozerskii Institute of Physicochemical Biology, Vorob'evy gory, Moscow State University, Moscow, 119899 Russia*

Received July 26, 1999

Abstract—Based on up-to-date physicochemical data, a complete kinetic model of the catalytic cycle of photosystem II (PS II) for higher green plants was constructed. In compliance with the time hierarchy of photosynthetic stages, the model was reduced in order to describe only processes occurring on the millisecond time scale. In terms of the model, chlorophyll fluorescence induction curves at different values of model parameters were calculated. The fluorescence intensity was determined from an equation for calculating the concentrations of PS II fluorescence states and their dependence on the components of the electrochemical potential across the tylacoid membrane. The proposed model, which considers only processes occurring within PS II, cannot describe some features of the ascending branch of the chlorophyll fluorescence induction curve. It was found that the steady-state level of the fluorescence intensity may nonmonotonically depend on the transmembrane electric potential.

INTRODUCTION

According to the current views, the primary (light-induced) stages of the photosynthesis in green plants are a set of electron-transport reactions proceeding in photosynthetic membranes of chloroplasts. These reactions involve a number of highly specialized integral membrane proteins [photosystems (PS) I and II and the b6/f cytochrome complex] and mobile electron carriers. In PS II, the electron transfer sequence and characteristic times of principal stages may be described as follows:

$$H_2O \xrightarrow{200\ ns} Chl \xrightarrow{3\ ps} Phe \xrightarrow{200\ ps} Q_A \xrightarrow{200\ \mu s} Q_B \xrightarrow{500\ \mu s} \ldots.$$

From the primary donor (H_2O), electrons are carried to the reacting site pigment P680 (Chl) and then to pheophytin (Phe) and to the primary and secondary quinone acceptors of electrons (Q_A and Q_B, respectively). Electron transfer along this route is accompanied by the generation of a transmembrane electrochemical potential $\Delta\mu_H$, which may be expended in the synthesis of adenosine triphosphate (ATP) and in the electrogenic leakage of H^+, K^+, Cl^-, and other ions through a tylacoid membrane. The kinetic mechanisms of regulation of these processes are normally studied by mathematical modeling. At the present time, there are many publications on models that describe electron transfer in separate fragments of the complex system of primary photosynthetic reactions. There are models of the superfast (10^{-12}–10^{-9} s) absorption of light, migration of electronic excited states, and primary charge separation [1–3], as well as models that describe slower (millisecond-scale) electron transfer processes involving the secondary quinone acceptor (Q_B) of PS II [4]. In [5], an attempt was undertaken to construct a joint model for the processes occurring on two different time scales. There are models that describe the interaction of two photosystems [6] and proton transport through the tylacoid membrane [7]. In all these models, photosynthetic reactions proceeding on a certain time scale are described in detail, while the description of the other stages is simplified. In most models, the dependence of the characteristics of the individual stages of the primary photosynthetic reactions on the transmembrane electric potential and the role of ionic (K^+, Cl^-, and other) fluxes through the tylacoid membrane are ignored. These fluxes may have a significant effect on parameters of primary photosynthetic reactions [2, 8, 9].

To verify a model of primary photosynthetic reactions, it is necessary to compare its predictions with experimentally observed effects. One of the quantitative criteria of adequacy of a model is its ability to describe inductive effects of photosynthesis, e.g., the chlorophyll fluorescence induction curve (Fig. 1), which is the time dependence of the intensity of the fluorescence from an object when an illumination is switched on after a period of dark adaptation. The so-called fast segment of the induction curve (*OIDP* segment), an increase in the fluorescence intensity within several seconds up to the maximum, was studied most thoroughly. According to the current notions, the specific features of this segment correspond to various processes occurring in the photosynthetic apparatus of the plant [8], such as an increase in the concentration of reduced quinone acceptor Q_A, an increase in the electric potential across the tylacoid membrane, and a change in the redox state of the plastoquinone pool. The

kinetic characteristics of segment *OIDP* was modeled in several works [3–6]. Based on these models, the authors explained the two-stage pattern of this segment of the induction curve.

We suggest a model of the primary photosynthetic processes in chloroplasts of higher green plants based on a detailed kinetic description of the catalytic cycles of the principal pigment–protein complexes involved in the system of light-induced reactions of photosynthesis. The model accounts for the dependence of the characteristics of a number of electron-transport processes on the electric potential difference and on the pH gradient across the tylacoid membrane.

In this work, we considered the block of the model that describes the catalytic cycle of PS II. We derived a function to describe dependence of the chlorophyll fluorescence intensity on the concentrations of a number of states of PS II and on the components of the electrochemical potential $\Delta\mu_H$ across the tylacoid membrane. The model does not describe the formation of $\Delta\mu_H$; its components (the transmembrane electric potential $\Delta\Psi$ and the proton gradient ΔpH) were given as parameters. This simplification made it possible to study internal regulatory properties of the PS II complex. An adequate description of the generation of $\Delta\mu_H$ requires, apart from PS II, a comprehensive study of the entire system of primary photosynthetic reactions. We examined the shape of the fluorescence induction curve at various electric potential differences and pH gradients across the tylacoid membrane. In addition, we studied the dependence of the steady-state fluorescence intensity on $\Delta\Psi$ and ΔpH.

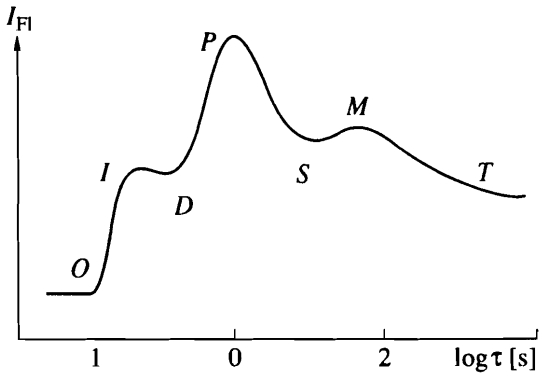

Fig. 1. Typical chlorophyll fluorescence induction curve for higher green plants with conventional designations of its kinetic phases. Segment *OIDP* segment refers to the so-called fast phase, and *PSMT*, to the slow phase of the induction curve. The fluorescence intensity is measured along the ordinate. The arrow shows the moment when light is switched on.

MATHEMATICAL MODEL

Complete mathematical model. In our model, the PS II complex is considered as a membrane enzyme that catalyzes the reduction of plastoquinone to plastoquinol and creates a transmembrane the proton electrochemical potential gradient $\Delta\tilde{\mu}_{H^+}$ under the action of light (Fig. 2). The mathematical model is given by the following system of differential equations:

$$d[\mathrm{PSII}_i]/dt = \sum_j v_{pj} - \sum_k v_{uk}, \qquad (1)$$

where $[\mathrm{PSII}_i]$ is the concentration of one of the states of the PS II complex, v_{pj} is the rate of production of PS II complexes in the jth reaction, and v_{uk} is the rate of consumption of PS II complexes in the kth reaction of the PS II catalytic cycle.

Here, PSII_i is determined by the state of its four electron carriers, i.e., P680 chlorophyll, pheophytin (Phe), the primary single-electron covalently bound quinone acceptors (Q_A), and the binding sites of the secondary plastoquinone acceptor (Q_B). According to the model, excitation energy, which is initially localized on one of the antenna pigments, is quickly (within several picoseconds) distributed throughout the entire pool of pigment molecules of the PS II antenna (including the P680 pigment of the reacting site) [1, 10]. Henceforward, the entire set of these pigments will be designated as Chl.

According to the current understanding of the electron transfer mechanism, each electron carrier involved in PS II can exist in several different states. P680 can exist in three states: reduced (Chl), excited (Chl*), and oxidized (Chl^+) (in this work, we do not consider the triplet state). Pheophytin and Q_A can exist in two states: oxidized (Phe and Q_A) and reduced (Phe^- and Q_A^-). The plastoquinone binding site (Q_B) can exist in four states: in complexes with plastoquinone (Q_B), semiquinone (Q_B^-), and deprotonated plastoquinone (Q_B^{2-}) and in an unfilled state, in which the site is bound with none of the Q_B forms. Thus, our model allows for $3 \times 2 \times 2 \times 4 = 48$ kinetic states of PS II. However, using available information about the rates and sequences of the primary photosynthetic reactions [10, 11], some of the hypothetical states of PS II can be excluded from consideration. It was found [8, 10] that the reduction of oxidized P680 by the water decomposition system (WDS) occurs faster (within 20–300 ns) than the electron transfer from Q_A to Q_B (200–400 μs). Therefore, the four states containing the $[Chl^+ \cdot Phe \cdot Q_A]$ fragment can be excluded from the model. In addition, an electron carried to pheophytin during the primary charge separation cannot be stabilized on it. It either returns to P680 (repopulation of the excited state) or is transferred to the primary quinone acceptor Q_A. Consequently, the PS II complex states containing the $[Chl \cdot Phe^-]$ and $[Chl^* \cdot Phe^-]$ combinations (16 states) can also be excluded from our consideration. Thus, the number of possible kinetic states of PS II can be reduced to 28. These states and possible transitions between them are

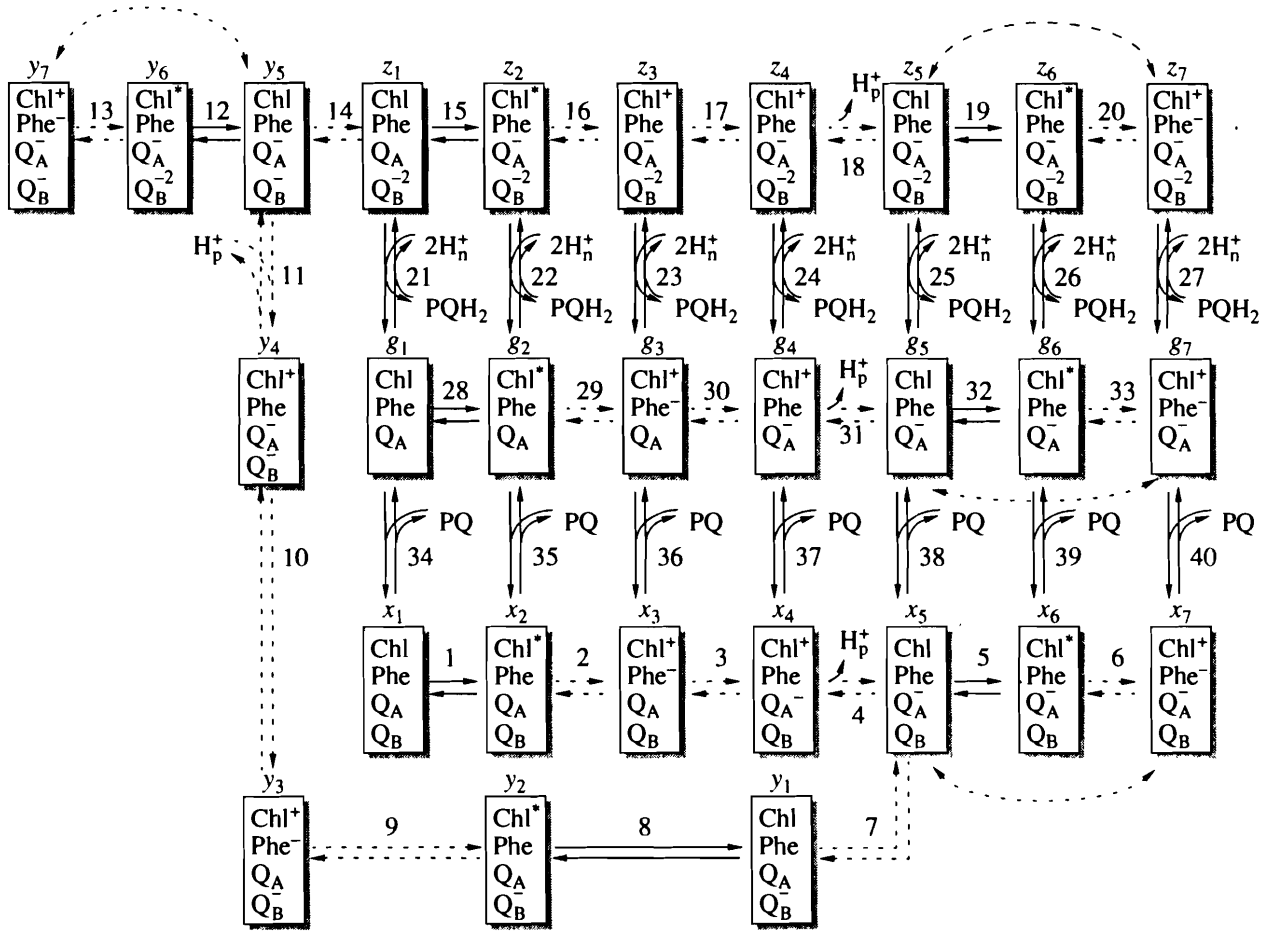

Fig. 2. Scheme of the full catalytic cycle for PS II. Each square represents one of the states of the PS II complex, which is determined by the redox states of the electron carriers involved: Chl (chlorophyll) is a complex composed of pigments of the PS II antenna, including the P680 pigment of the reacting site; Phe (pheophytin) is the primary acceptor of electrons; Q_A and Q_B are the primary and secondary quinone acceptors of electrons. The superscripts x_i, y_i, z_i, g_i ($i = 1, \ldots, 7$) over the squares denote model variables. Dashed arrows show fast (characteristic times lesser than 0.1 ms) steps; solid arrows indicate slow (characteristic times no lesser than 1 ms) steps. Numbers near the arrows correspond to the numbers of the stages; PQ is plastoquinone; PQH_2 is plastoquinol; H_p^+ denotes protons released into the intratylacoid space; and H_n^+ denotes protons absorbed from the tylacoid stroma.

shown in a diagram of the complete catalytic cycle of PS II (Fig. 2).

After a prolonged dark adaptation, P680 is completely reduced, whereas pheophytin and Q_A are oxidized. Thus, before exposure to light, PS II can exist only in two states (x_1 and g_1), which are at equilibrium [via reaction (34)]. The equilibrium concentrations of these states are determined by the constant of binding and the total concentration of plastoquinone (PQ) in the membrane. Upon exposure to light, P680 passes into the excited state (x_2, g_2) [reactions (1) and (28), respectively] with a subsequent transfer of an electron to pheophytin [reactions (2) and (29)]; i.e., the process of primary charge separation occurs. Since the electron can not be stabilized on pheophytin, it is carried further to Q_A [reactions (3) and (30)]. Then WDS donates an electron to the oxidized pigment, thereby bringing it to the initial (reduced and unexcited) state (x_5 and g_5). Every four events of reduction of oxidized P680 by WDS are accompanied by the decomposition of two H_2O molecules, liberation of one molecule of oxygen and four H_p^+ protons into the intratylacoid space, which thus becomes positively charged. In our model, the molecular mechanism of functioning of WDS was not considered; it was assumed that one proton is liberated into the intratylacoid space per each electron carried from WDS to oxidized P680 [reactions (4) and (31)].

Thus, the sequence of steps (1)–(4) or (28)–(31) results in the formation of so-called closed reaction sites (RS) with reduced Q_A (states x_5 and g_5). Further exposure of closed RS to light may lead to a reexcitation of the pigment [reactions (5) and (32)] and to the process of primary charge separation [reactions (6) and (33)]. As a result, PS II states with oxidized pigment

and reduced pheophytin and Q_A are formed (x_7 and g_7). At present, there are different opinions about further transformations of these states. The unstable charge on the pheophytin Phe^- can recombine with an electron hole on $P680^+$ in two ways: it may repopulate the P680* excited states (transitions of states with a subscript 7 to those with a subscript 6) or the ground state via a nonradiative recombination of the primary pair (transitions of states with subscript 7 to those with subscript 5, as shown in the diagram with broken arrows without numbers). For any of the g_i states (i =1, ..., 7), the binding of plastoquinone (PQ) with PS II Q_B sites may take place [reactions (34)–(40)], resulting in the formation of the corresponding x_i states (i = 1, ..., 7). The bound plastoquinone is a two-electron carrier; therefore, it can accept successively two electrons from Q_A^- [transfer of the first electron from Q_A^- to Q_B is described by reaction (7)].

Further exposure is accompanied by events developing according to the above-described scenario: the excitation of the pigment [reaction (8)], primary charge separation [reaction (9)], stabilization of an electron on Q_A [reaction (10)], reduction of oxidized P680 by WDS [reaction (11)], excitation of a closed RS of PS II with reduced Q_A [reaction (12)], and primary charge separation [reaction (13)] with a possible recombination of the primary radical pair [back reaction (13) and unnumbered stage designated by the dashed line]. Reaction (14) involves transfer of an electron from Q_A^- to semiquinone of the Q_B site with the formation of the completely deprotonated plastoquinone Q_B^{2-}. Further exposure results in the already twice described sequence of events in PS II, where deprotonated plastoquinone is bound at Q_B sites (the corresponding states of PS II are designated as z_i [i = 1, ..., 7]); the process results in the reduction of Q_A [reactions (15)–(20)]. In parallel, in each of the z_i (i = 1, ..., 7) states, the plastoquinone PQH_2 can be released with a preliminary absorption of two H_n^+ protons from the chloroplast stroma (that becomes negatively charged) and formation of the initial states g_i (i = 1, ..., 7); the Q_B site is left unfilled [reactions (21)–(27)]. Thus, the catalytic cycle of PS II is accomplished.

The x_i, y_i, z_i, and g_i values (i = 1, ..., 7) are model variables; they are determined by a system of differential equations of form (1), which corresponds to the scheme of the PS II catalytic cycle shown in Fig. 2. The concentrations of protons in the intratylacoid space (H_p^+) and in the chloroplast stroma (H_n^+), the electric potential difference across the tylacoid membrane ($\Delta\Psi$), and the intramembrane concentrations of plastoquinone and plastoquinol are model parameters. Reaction rates are given in compliance with the law of mass action and are functions of the variables and parameters of the model. For a detailed description of each reaction, one should only know its equilibrium constant and one of the rate constants (either for a direct or the back reaction):

$$K_i = k_i/k_{-i}. \quad (2)$$

Exposure to light affects the redox states of electron carriers and, consequently, their conformations and, possibly, electron transfer rate constants [12]. In this work, this effect was not taken into account. The equilibrium constants of the redox reactions were determined from experimentally measured midpoint redox potentials:

$$K = \exp\left(\frac{\Delta E_m}{RT/nF}\right). \quad (3)$$

Here, ΔE_m is the difference between the midpoint redox potentials measured with respect to a standard hydrogen electrode, F is the Faraday constant, and n is the number of electrons carried in the course of a redox reaction.

Stages (1), (5), (8), (12), (15), (19), (28), and (32) are light-induced reactions; they describe the transition of Chl into the excited state Chl* (constants k_{Li}, i = 1, 5, 8, 12, 15, 19, 28, and 32) and the inverse process of deactivation of the excited state (constants χ_i, i = 1, 5, 8, 12, 15, 19, 28, and 32). The values of k_{Li} are proportional to the light intensity [13, 14]: $k_{Li} \sim I\sigma$, where I is the light intensity and σ is the effective absorption cross section of PS II. In the absence of light, all these constants equal zero; at a light intensity of 10^3 W/m^2 (light intensity from the Sun in zenith), $k_{Li} \sim 10^3$ s^{-1}.

The deactivation of the Chl* excited states into the ground state is accompanied by a fluorescence (other, less effective, pathways of Chl* deactivation are also possible). In our model, the function for calculating the fluorescence intensity was represented as a sum of the concentrations of the PS II fluorescent states (with excited Chl*) multiplied by the relevant fluorescence constants χ_i:

$$I_{Fl} = \chi_1\chi_2 + \chi_8 y_2 + \chi_{15} z_2 + \chi_{28} g_2 + \chi_5 x_6 + \chi_{12} y_6 + \chi_{19} z_6 + \chi_{32} g_6. \quad (4)$$

The kinetic scheme under study contains cycles where the initial and final states are equal, for example, the cycle ($z_1 - z_2 - g_2 - g_1 - z_1$). According to the condition of detailed balance [15], the product of the equilibrium constants along the coordinate of reactions of this cycle should be equal to unity. Thus, there is the following restriction on the rate and equilibrium constants for the reactions of this cycle:

$$\chi_{28} = \frac{k_{L28}}{k_{L15}}\chi_{15}. \quad (5)$$

The kinetic scheme (Fig. 2) contains 12 cycles; therefore, eleven equations of detailed balance should be additionally introduced.

Each stage involving electric charge transfer through the membrane produces a membrane potential $\Delta\Psi$, which, in turn, affects the equilibrium and rate constants of all electrogenic stages [16–18]:

$$K_{eq}(\Delta\Psi) = \exp[-\alpha\Delta\Psi/(RT/F)]K_{eq},$$
$$k_+(\Delta\Psi) = \exp[-\delta\alpha\Delta\Psi/(RT/F)]k_+, \quad (6)$$
$$k_-(\Delta\Psi) = \exp[(1-\delta)\alpha\Delta\Psi/(RT/F)]k_-.$$

Here, $\alpha\Delta\Psi$ is the membrane potential generated by the stage in question during charge transfer through the membrane, and δ is the component of the membrane potential $\alpha\Delta\Psi$ that affects the rate constant of the direct reaction.

Reduced mathematical model. According to the current notions about the rates of separate stages of the PS II catalytic cycle, all processes depicted in Fig. 1 can be qualified as fast (characteristic times less than 0.1 ms) or slow (characteristic times no less than 1 ms). Light-induced stages involving the adsorption of light quanta by Chl are slow reactions: P680 passes into the excited state [reactions (1), (5), (8), (12), (15), (19), (28), and (32)], plastoquinone is bound [reactions (34)–(40)], and plastoquinol dissociates [reactions (21)–(27)]. The remaining reactions are fast. In accordance with the Tikhonov theorem [19], we treated all fast reactions as quasi-stationary processes; as a result, we reduced the system of 28 equations that describes the PS II catalytic cycle to a system containing 10 equations. In so doing, we neglected the stages that describe the nonradiative recombination of charges in the primary radical pair (shown in Fig. 2 by unnumbered broken arrows), because we assumed that their effectiveness is considerably lower than that of the radiating recombination reactions.

Passing to the limit with respect to the rate constants of the fast reactions and substituting the variables as

$$\mathrm{PSII}_0 = g_1, \quad \mathrm{PSII}_1 = x_1, \quad \mathrm{PSII}_2 = \sum_{i=2}^{5} x_i + y_1,$$
$$\mathrm{PSII}_3 = \sum_{i=2}^{5} y_i + z_1, \quad \mathrm{PSII}_4 = \sum_{i=2}^{5} z_i, \quad (7)$$
$$\mathrm{PSII}_5 = \sum_{i=2}^{5} g_i, \quad \mathrm{PSII}_6 = x_6 + x_7,$$
$$\mathrm{PSII}_7 = y_6 + y_7, \quad \mathrm{PSII}_8 = z_6 + z_7, \quad \mathrm{PSII}_9 = g_6 + g_7,$$

we obtain a system of equations with new variables for PSII_i ($i = 0, \ldots, 9$). This scheme corresponds to the kinetic scheme shown in Fig. 3. The effective rate constants of the reduced model $\rho_{\pm i}$ ($i = 1, \ldots, 14$) are functions of the light constants; rate constants for the processes of fluorescence, plastoquinone binding, and plastoquinol dissociation; constants of equilibrium for the fast reactions of the complete model; electric potential difference; and the concentration of protons within the tylacoid membrane. Transforming the equation for $\rho_{\pm i}$ so that the numerator would be on the order of k_L and neglecting the terms smaller than 10^{-3} in the denominator, we have the following equations:

$$\rho_1 = k_{L1},$$
$$\rho_{-1} = (10^4\chi_{15}k_{L1}/k_{L15})/(K_2^0K_3^0K_4^0(K_7+1)$$
$$\times \exp[-(\delta_{II}^1+\delta_{II}^2+\delta_{II}^3)\varphi]$$
$$+ [H_p^+]\times 10^4K_2^0K_3^0\exp[-(\delta_{II}^1+\delta_{II}^2)\varphi]),$$
$$\rho_2 = k_{L8}/\left(1+\frac{1}{K_7}+[H_p^+]\times 10^4\frac{\exp(\delta_{II}^3\varphi)}{K_4^0K_7}\right),$$
$$\rho_{-2} = (10^4\chi_8)/(K_9^0K_{10}^0K_{11}^0(K_{14}+1)$$
$$\times \exp[-(\delta_{II}^1+\delta_{II}^2+\delta_{II}^3)\varphi]$$
$$+ [H_p^+]\times 10^4K_9^0K_{10}^0\exp[-(\delta_{II}^1+\delta_{II}^2)\varphi]),$$
$$\rho_3 = \frac{\chi_H^0\exp(-\delta_{II}^4d\varphi)}{1+1/K_{14}+[H_p^+]\times 10^4\exp(\delta_{II}^3\varphi)/K_{11}^0K_{14}},$$
$$\rho_{-3} = \chi_{-H}^0\exp[\delta_{II}^4(1-d)\varphi], \quad 0\le d\le 1,$$
$$\rho_4 = \chi_Q, \quad \rho_{-4} = \chi_{-Q},$$
$$\rho_5 = k_{L15}/\left(1+\frac{1}{K_{14}}+[H_p^+]\times 10^4\frac{\exp(\delta_{II}^3\varphi)}{K_{11}^0K_{14}}\right),$$
$$\rho_{-5} = (10^4\chi_{15})/(K_2^0K_3^0K_4^0(K_7+1)$$
$$\times \exp[-(\delta_{II}^1+\delta_{II}^2+\delta_{II}^3)\varphi] + [H_p^+]$$
$$\times 10^4K_2^0K_3^0\exp[-(\delta_{II}^1+\delta_{II}^2)\varphi]),$$
$$\rho_6 = \chi_H^0\exp(-\delta_{II}^4d\varphi),$$
$$\rho_{-6} = \chi_{-H}^0\exp(\delta_{II}^4(1-d)\varphi), \quad 0\le d\le 1,$$
$$\rho_7 = k_{L28},$$
$$\rho_{-7} = (10^4\chi_{15}k_{L28}/k_{L15})/(K_2^0K_3^0K_4^0(K_7+1)$$
$$\times \exp[-(\delta_{II}^1+\delta_{II}^2+\delta_{II}^3)\varphi]$$
$$+ [H_p^+]\times 10^4K_2^0K_3^0\exp[-(\delta_{II}^1+\delta_{II}^2)\varphi]),$$
$$\rho_8 = \chi_Q,$$
$$\rho_{-8} = \frac{\chi_{-Q}[1/K_7+[H_p^+]\times 10^4\exp(\delta_{II}^3\varphi)/K_4^0K_7]}{1+1/K_7+[H_p^+]\times 10^4\exp(\delta_{II}^3\varphi)/K_4^0K_7},$$

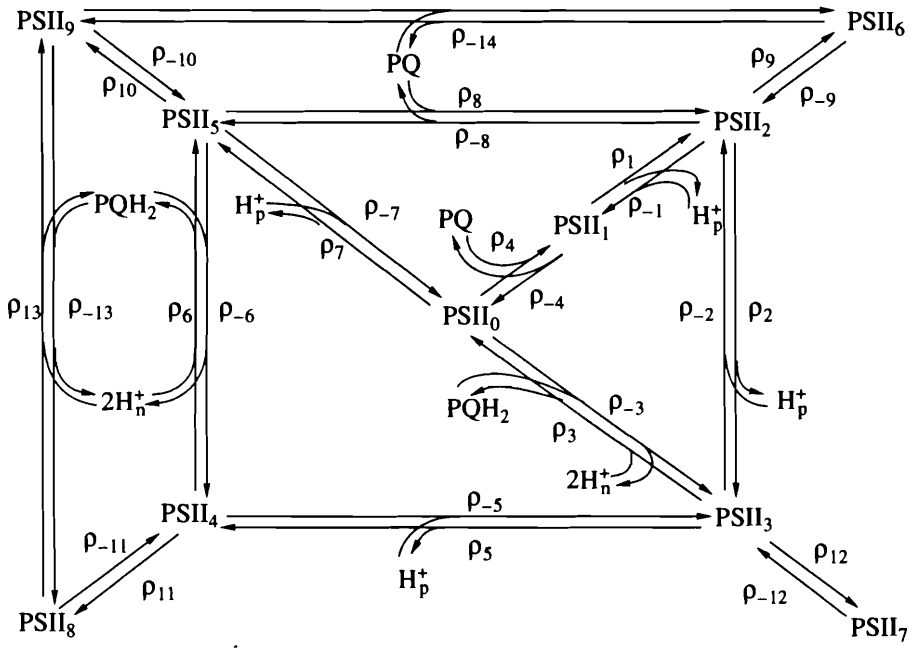

Fig. 3. Reduced scheme of the PS II catalytic cycle. $PSII_i$ ($i = 0, \ldots, 9$) denotes model variables derived from the complete model of the PS II catalytic cycle via the reduction of the fast processes; $\rho_{\pm i}$, ($i = 1, \ldots, 14$) are the effective rate constants that are functions of the rate constants of the complete catalytic cycle. Equations for $PSII_i$ and $\rho_{\pm i}$ are given in the text. For the other designations, see Fig. 2.

$$\rho_9 = \frac{k_{L5}}{1 + K_7 + [H_p^+] \times 10^4 \exp(\delta_{II}^3 \varphi)/K_4^0},$$

$$\rho_{-9} = \frac{\chi_{19} k_{L5}/k_{L19}}{K_6^0 \exp(-\delta_{II}^1 \varphi)},$$

$$\rho_{10} = \frac{k_{L32}}{1 + [H_p^+] \times 10^4 \exp(\delta_{II}^3 \varphi)/K_4^0},$$

$$\rho_{-10} = \frac{\chi_{19} k_{L32}/k_{L19}}{K_6^0 \exp(-\delta_{II}^1 \varphi)},$$

$$\rho_{11} = \frac{k_{L19}}{1 + [H_p^+] \times 10^4 \exp(\delta_{II}^3 \varphi)/K_4^0},$$

$$\rho_{-11} = \frac{\chi_{19}}{K_6^0 \exp(-\delta_{II}^1 \varphi)},$$

$$\rho_{12} = \frac{k_{L12}}{1 + K_{14} + [H_p^+] \times 10^4 \exp(\delta_{II}^3 \varphi)/K_{11}^0},$$

$$\rho_{-12} = \frac{\chi_{12}}{K_{13}^0 \exp(-\delta_{II}^1 \varphi)},$$

$$\rho_{13} = \chi_H^0 \exp(-\delta_{II}^4 d\varphi),$$

$$\rho_{-13} = \chi_{-H}^0 \exp[\delta_{II}^4 (1-d)\varphi],$$

$$\rho_{14} = \chi_Q, \quad \rho_{-14} = \chi_{-Q}.$$

The formula for calculating the fluorescence intensity is obtained by substituting the relationships of the old variables (x_i, y_i, z_i, and g_i; $i = 1, \ldots, 6$) through the new variables ($PSII_i$, where $i = 2, \ldots, 9$) into Eq. (4).

The results that follow were obtained by a numerical solution of the system of kinetic equations corresponding to the kinetic scheme shown in Fig. 3 (reduced model). The system describes the kinetic behavior of PS II that lacks stages responsible for nonradiative recombination of charges on the millisecond time scale. The steady-state values of the model variables were calculated from the corresponding system of algebraic equations, which were obtained by equating the right-hand side of each equation to zero. This system was solved with the use of the SCAMP software package.

Some of the model parameters were chosen on the basis of the data (equilibrium and rate constants) reported in [11, 13, 14]; the other parameters were varied [light constants k_{Li}, concentrations of protons in the lumen (H_p^+) and stroma (H_n^+), and electric potential difference $\Delta\Psi$]. A complete description of the model parameters is given below.

(A) The equilibrium constants for the processes of primary charge separation $K_2^0 = K_6^0 = K_9^0 = K_{13}^0 = K_{16}^0 = K_{20}^0 = K_{29}^0 = K_{33}^0 = 3 \times 10^6$ (The numbers of the constants correspond to the numbers of the stages in Fig. 2.) (B) The equilibrium constants for the electron transfer from Phe^- to Q_A: $K_3^0 = K_{10}^0 = K_{17}^0 = K_{30}^0 = 5 \times$

10^7. (C) The equilibrium constants for the reduction of $P680^+$ by WDS: $K_4^0 = K_{11}^0 = K_{18}^0 = K_{31}^0 = 50$. (D) The equilibrium constant for the transfer of the first electron from Q_A^- to Q_B: $K_7^0 = 20$. (E) The equilibrium constant for the transfer of the second electron from Q_A^- to Q_B^-: $K_{14}^0 = 10$. (F) The fluorescence constants: $\chi_i = 10^9\ s^{-1}$, $i = 1, 5, 8, 12, 15$. (G) The constants describing the binding of plastoquinone with PS II Q_B sites [reaction (34)–(40)]: $\chi_{-Q} = 50$, $\chi_Q = 500$. (H) The constants characterizing the release of protonated plastoquinone from PS II Q_B sites and the constants for the corresponding reverse reactions [stages (21)–(27)]: $\chi_H^0 = 10^{10}$ and $\chi_{-H}^0 = 0.4$. (I) The components of the transmembrane electric potential $\Delta\Psi$ created by the individual stages of the PS II catalytic cycle: for the process of primary charge separation, $\delta_{II}^{(1)} = 0.6$; for the transfer of an electron onto the quinone acceptor Q_A, $\delta_{II}^{(2)} = 0.2$; for the reduction of the reacting site pigment, $\delta_{II}^{(3)} = 0.1$; for the protonation of the secondary quinone acceptor Q_B^{2-}, $\delta_{II}^{(4)} = 0.1$. (J) The component of the membrane potential that affects the rate constant for the direct reaction: $d = 0.5$.

RESULTS AND DISCUSSION

Based on the experimentally measured characteristic times and midpoint potentials for the redox pairs of the electron transfer stages, we constructed two models (full and reduced) for the functioning of PS II, i.e., the light-induced transfer of electrons from the water decomposition system to plastoquinone and the reduction of plastoquinone to plastoquinol. The reduced PS II model describes only the processes whose characteristic time is no less than hundreds of microseconds. All light-induced stages of the excitation of P680 [reactions (1), (5), (8), (12), (15), (19), (28), and (32)], plastoquinone binding [reactions (34)–(40)], and plastoquinol dissociation [reactions (21)–(27)] were attributed to slow reactions. The rest of the reactions were assumed to be fast. The model takes into account the dependence of the characteristics of the electrogenic stages (electron or proton transfer) on the electric potential. However, in this work, we did not study variations in $\Delta\mu_H$; the components of the electrochemical potentials created by protons ($\Delta\Psi$ and ΔpH) were fixed model parameters. This approach makes it possible to study the regulatory properties of the PS II complex, which are independent of variations in $\Delta\Psi$ or ΔpH and, consequently, can be regarded as internal regulatory properties.

The complete model that describes both the fast and slow stages of the PS II catalytic cycle can be applied to correctly describe the fast fluorescence and to predict of the states of the photosynthetic apparatus arising under the action of various factors (for example, on the basis of the fluorescence parameters F_0 and F_{max}). In addition, the complete model can be used in describing pulse fluorometry experiments and the kinetic characteristics of PS II. We applied the reduced model to describing the fast stage of the chlorophyll fluorescence induction. The observed effect is an increase in the fluorescence intensity of an object in response to illumination after a period of dark adaptation during several seconds (Fig. 1). Most of the models of this phenomenon were confined to processes occurring in PS II [3–5]. The authors justify this simplification by the argument that the fluorescence measured while recording induction curves is practically restricted to PS II.

One of the goals of this work was to verify whether it is possible to explain the observed two-phase behavior of *OIDP* in the framework of the regulatory properties of PS II. We tried to find out whether the fluorescence induction curve predicted by our model would exhibit a characteristic nonmonotonic pattern (local maximum *D* or at least plateau *OID* in Fig. 1) in the 50- to 500-ms range, as is the case with the experimentally obtained curves. For that purpose, we studied model curves of fluorescence induction with varying parameters of the model. Each curve of the fluorescence induction was predicted for the PS II fluorescence yield [see formula (4)] as a function of time under the action of light of constant intensity after a period of dark adaptation.

The initial conditions were formulated based on the assumption that on a dark adaptation of the object occurs: $[PSII_1] = 1.612$ mM; $[PSII_0] = 0.008$ mM; $[PSII_i] = 0$ ($i = 2, 3, \ldots, 9$); the concentration of plastoquinone [PQ] = 19 mM; the concentration of protonated plastoquinol $[PQH_2] = 1$ mM; the concentrations of protons in the lumen and stroma H_p^+ and H_n^+ and the electric potential difference $\Delta\Psi$ were varied from 10^{-5} to 10^{-8} M and from 0 to 200 mV, respectively.

The results show that the curve of fluorescence induction has a characteristic S-shaped form at all values of the model parameters. No two-stage quick fluorescence rise was observed. Variations in the model parameters lead only to changes in the stationary level of the fluorescence intensity and sometimes in the rate of approaching this level. An increase in the light constant k_L results in an increase in the stationary fluorescence intensity and in a shortening of the time of reaching it (Fig. 4a). By contrast, the acidification of the stroma and intratylacoid space, a process that affects the proton gradient difference ΔpH equal to 2 ($pH_n = 8$, $pH_p = 6$), results in a decrease in the stationary level of the fluorescence intensity. An increase in the electric potential across the tylacoid membrane $\Delta\Psi$ has a lim-

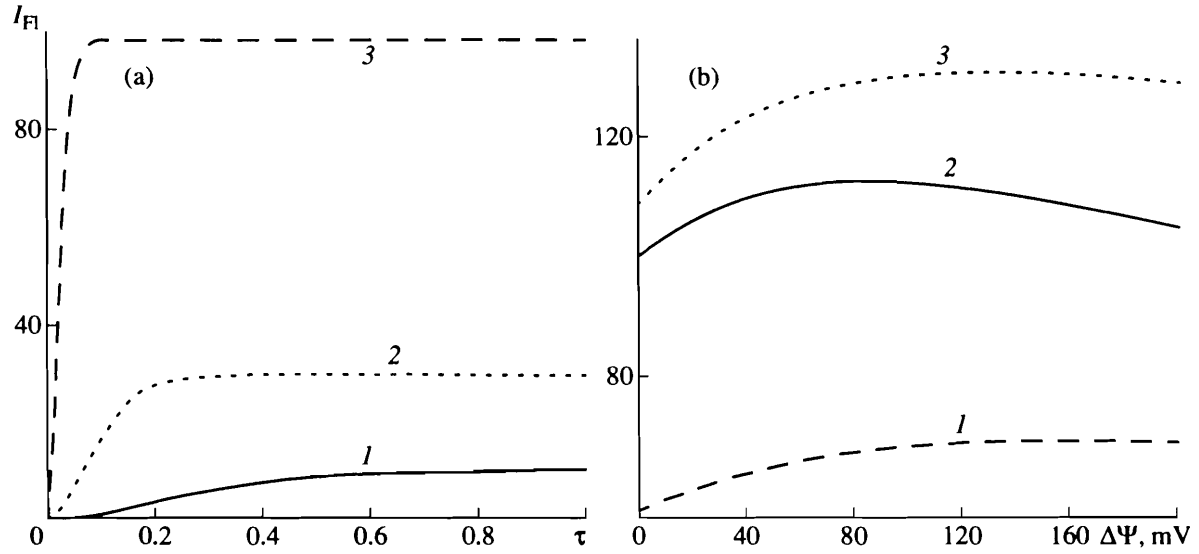

Fig. 4. Results of modeling of the chlorophyll fluorescence induction by the reduced model for the PS II catalytic cycle: (a) fluorescence induction curves obtained under various conditions of illumination; light constant k_L = (*1*) 10, (*2*) 30, and (*3*) 100; (b) the dependence of the steady-state fluorescence intensity on the electric potential difference across the tylacoid membrane calculated at various values of the transmembrane proton gradient ΔpH and pH in the lumen [pH_p (*1*, *2*) 6 and (*3*) 6.5] and tylacoid stroma [pH_n (*1*) 6.5 and (*2*, *3*) 8]. For the other model parameters, see the text.

ited effect on the steady-state fluorescence intensity. As can be seen from Fig. 4b, this dependence is bell-shaped; i.e., the optimum ΔΨ value corresponding to the maximum fluorescence intensity exists at constant values of the model parameters. A deviation from the optimum ΔΨ results in a decrease in the fluorescence intensity. A nonmonotonic dependence of the stationary fluorescence intensity on ΔΨ can be explained by the fact that light intensities close to the saturating level ($10 < k_L < 100$), the principal source of PS II fluorescence, are associated with the state z_6 (Fig. 2), which corresponds to the reduced Q_A and plastoquinol at the Q_B site. The stationary concentration of this form depends on ΔΨ, because the reactions yielding it [(16)–(18)] and the reaction consuming z_6 (step 26) depend on ΔΨ. Since reactions (16)–(18) describe the path of charges almost through the entire membrane, while reaction (26) involves only charge (proton) transfer from the stroma to the Q_B site, the processes of generation of z_6 more strongly depend on ΔΨ. Since this dependence is exponential, we may suppose that, at low ΔΨ, the rate of reaction (26) decreases to a greater extent those of reactions (16)–(18); by contrast, at high ΔΨ, the rates of reactions (16)–(18) are predominantly decreased. Figure 4b shows that oxidation of the intratylacoid space (a decrease in pH_p) shifts the fluorescence intensity maximum to the left, whereas the oxidation of the stroma (a decrease in pH_n), to the right.

A monotonic character of the fluorescence induction curves predicted by the model is a result of the simplifications we made. In fact, we did not introduce the step of formation of the transmembrane potential $\Delta\mu_H$; its components (ΔΨ and ΔpH) were given as model parameters. A nonmonotonic behavior of fluorescence in the *OIDP* segment may be accounted for by involvement of PS II in other primary photosynthetic processes, such as the formation of the electrochemical potential on the tylacoid membrane and transmembrane ionic flows. There are data that the membrane potential may affect the fluorescence yield through changes in the energy levels of the PS II intermediate states, which in turn cause changes in the rate constants of fast reactions of electron transport [2, 20]. Results of modeling the kinetics of generation of the transmembrane electrochemical potential and its effect on the pattern of initial stages of the fluorescence induction curve will be discussed in a future publication.

ACKNOWLEDGMENTS

This work was supported by the Russian Foundation for Basic Research, project nos. 98-04-48868, 98-07-90097, 00-04-48919.

REFERENCES

1. Schatz, G.H., Brock, H., and Holzwarth, A.R., *Biophys. J.*, 1988, vol. 54, p. 397.
2. Leibl, W., Breton, J., Deprez, J., and Trissl, H.W., *Photosynth. Res.*, 1989, vol. 22, p. 257.
3. Trissl, H.-W., Gao, Y., and Wulf, K., *Biophys. J.*, 1993, vol. 64, p. 974.
4. Renger, G. and Shulze, A., *Photobiochem. Ptotobiophys.*, 1985, vol. 9, p. 79.
5. Baake, E. and Shloeder, J.P., *Bull. Math. Biol.*, 1992, vol. 54, p. 999.

6. Kukushkin, A.K. and Tikhonov, A.N., *Lektsii po biofizike fotosinteza vysshikh rastenii* (Lectures on the Biophysics of Photosynthesis in Higher Plants), Moscow: Mosk. Gos. Univ., 1988.
7. Dubinskii, A.Yu. and Tikhonov, A.N., *Biofizika*, 1994, vol. 39, no. 4, p. 652.
8. Dau, H., *J. Photochem. Photobiol., B*, 1994, vol. 26, p. 3.
9. Van Kooten, O., Snel, J.F.H., and Vredenberg, W.J., *Photosynth. Res.*, 1986, vol. 9, p. 211.
10. Dau, H., *Photochem. Photobiol.*, 1994, vol. 60, p. 1.
11. Hall, D.O. and Rao, K.K., *Photosynthesis. Studies in Biology*, Cambrige: Cambrige Univ., 1994, 5th ed.
12. Rubin, A.B., Kononenko, A.A., Shaitan, K.V., *et al.*, *Biofizika*, 1994, vol. 39, no. 2, p. 213.
13. Molecular Mechanism of Energy Transformation in the Primary Process of Photosynthesis, *Itogi Nauki Tekh., Ser. Biofizika*, Moscow: VINITI, 1987, vol. 20.
14. Principles of Regulation and Model Systems of Primary Photosynthesis Processes, *Itogi Nauki Tekh., Ser. Biofizika*, Moscow: VINITI, 1987, vol. 22.
15. Westerhoff, H.V. and Van Dam, K., *Thermodynamics and Control of Biological Free-Energy Transduction*, Amsterdam: Elsevier, 1987.
16. Skulachev, V.P. and Kozlov, I.A., *Protonnye adenozintrifosfatazy: molekulyarnye biologicheskie generatory toka* (Protonic Adenosine Triphosphates: Molecular Biological Electric Current Generators), Moscow: Nauka, 1977.
17. Reynolds, I.A., Johnson, E.A., and Tanford, C., *Proc. Natl. Acad. Sci. USA*, 1985, vol. 82, p. 6869.
18. Demin, O.V., Vesterkhoff, Kh.V., and Kholodenko, V.N., *Biokhimiya*, 1998, vol. 63, p. 755.
19. Tikhonov, A.N., *Mat. Sb.*, 1952, vol. 31, no. 3, p. 575.
20. Dau, H., Windecker, R., and Hansen, U.P., *Biochim. Biophys. Acta*, 1991, vol. 1057, p. 337.